# Ordered TiO$_2$ nanotubes: The effect of preparation parameters on the photocatalytic activity in air purification process

Michał Nischk [a], Paweł Mazierski [a], Maria Gazda [b], Adriana Zaleska [a],*

[a] Department of Chemical Technology, Faculty of Chemistry, Gdansk University of Technology, 80-233 Gdansk, Poland
[b] Department of Solid State Physics, Faculty of Applied Physics and Mathematics, Gdansk University of Technology, 80-233 Gdansk, Poland

## ARTICLE INFO

## ABSTRACT

Vertically ordered TiO$_2$ nanotube arrays were synthesized by anodic oxidation of titanium foil in glycerol, ethylene glycol and water-based electrolytes. The effect of electrolyte composition, anodization voltage, ultrasonic treatment and calcination time on the morphology of the resulting thin films, as well as on their photocatalytic activity in toluene removal, used as a model volatile organic compound, was investigated. Toluene, at the concentration of about 100 ppm, was irradiated over TiO$_2$ nanotube arrays using xenon lamp and light-emitting diodes (LEDs) in four subsequent cycles. The results showed that toluene could be mostly removed from the air after 30 min of irradiation over TiO$_2$ nanotubes (NTs), even using LEDs (375 nm) as a irradiation source. Photoactivity increased with increasing of nanotubes lengths and decreasing of crystallite size. Thus, TiO$_2$ nanotube arrays formed in ethylene glycol-based electrolyte by applying voltage of 40 V, followed by 1-h calcination at 450 °C, revealed the highest photoactivity and may be used several times without any significant decrease in activity.

## 1. Introduction

Air pollutants such as chemicals, particulate matter and biological materials cause harm and discomfort to humans and other living organisms. Major chemicals, known as air pollutants and produced by human activity, include: sulfur dioxide (SO$_2$), nitrogen oxides (NO$_x$), volatile organic compounds (VOCs) and pathogenic microorganisms. Among to the others methods, heterogeneous photocatalysis has been proposed to remove both organic and inorganic compounds together with microorganisms from outdoor and indoor air. TiO$_2$ materials were used to degrade compounds such as: trichloroethylene, methanol, benzene [1], toluene [2,3], acetone, ethanol [3], acetaldehyde [4], carbon monoxide, nitric oxides [5], mixture of different VOCs [6] and also a pathogenic microorganisms, like *Legionella pneumophila* bacteria [7]. Different geometry and construction of the reactors were used to perform photocatalytic air purification process [8,9]. Commercially available P25 TiO$_2$ was the most widely investigated and used photocatalyst for air purification processes [1,3,4,10]. Another TiO$_2$ photocatalyst was obtained via chemical vapor deposition of TiO$_2$ precursor (titanium tetraisopropoxide) [11]. Based on the literature data and own experience, it could be concluded that the efficiency of the photocatalytic air treatment system depends on three basis parameters: (a) activity of the photocatalyst, (b) surface area of the photocatalyst (e.g. surface area of photocatalyst support), and (c) type and power of irradiation source. Thus, one of the challenges in the field of photocatalytic air treatment systems is the development of photoactive materials, in the form of thin layer, activated by low powered and low cost irradiation sources (such as LEDs) to remove VOCs, microorganism and to deodorize air streams. Nanotubes arrays meet these requirement, since they can be directly grown on a support material and posses high surface area, which guarantee enhanced photon absorption together with an extensive adsorption of reactant molecules on the photocatalyst surface [12]. Furthermore, TiO$_2$ NTs possess a number of attractive properties, such as potentially enhancing electron percolation pathways, light conversion, as well as improved ion diffusion at the semiconductor–electrolyte interface [13]. TiO$_2$ nanotubes, due to their unique features, could be used as photocatalytic material, in solar cells, in electrochromic devices, as a biomedical coating, drug-delivery capsule and biosensors [14].

The morphological structure of anodized TiO$_2$ nanotubes as well as their photocatalytic activity can be modified by changing preparation conditions, like anodization time, applied voltage, temperature, Ti foil roughness, calcination parameters and electrolyte composition including fluoride concentration, solvent, water content, pH, viscosity, conductivity, and organic additives [15,16]. According to Zhang et al. [17] there are several generations of TiO$_2$ nanotubes produced via anodic oxidation. First generation nanotubes were obtained by titanium anodization in an aqueous electrolyte containing fluorides, i.e. 1 M H$_2$SO$_4$ + 0.15 wt% HF [18] or 0.5 M H$_3$PO$_4$ + 0.14 M NaF [19]. The second generation

* Corresponding author. Tel.: +48 583472437; fax: +48 583472065.
  *E-mail address:* adriana.zaleska@pg.gda.pl (A. Zaleska).

nanotubes are fabricated using organic-based electrolytes, such as ethylene glycol + 10 wt% $H_2O$ + 0.135 M $NH_4F$ [20] or 55% (v/v) glycerol + 45% (v/v). $H_2O$ + 0.27 M $NH_4F$ [21]. $TiO_2$ nanotube arrays of different lengths were prepared by electrochemical anodization of titanium disks in $NH_4F$–$H_2O$–formamide solution, followed by annealing at 450 °C and used for water splitting [12]. A square-shaped fast photoresponse was recorded with ordered and fully top-open nanotubular structures. On the other hand, clogged tubes not only yielded low current densities, but also showed delayed photocurrent transient signals due to the reduced mobility of the charge carriers within the preferentially oriented anatase layer [12]. Recently, it was demonstrated that $TiO_2$ nanotube arrays can indeed have a higher photocatalytic reactivity than a comparable nanoparticulate layer [22] and it was shown that $TiO_2$ NTs doped with small amounts of Ru, Nb or Ta [23–25] dramatically enhanced water-splitting. However, there is only a few reports about using anodized, ordered TNTs arrays as a photocatalytic material for air treatment. $TiO_2$ NTs were used to remove acetalaldehyde [26], toluene and benzene [27] and $NO_x$ oxidation [28] in the gas phase.

Although the $TiO_2$ NTs have been studied intensively for water splitting, to our best knowledge, there has been no report on using UV-light-emitting diodes for gas phase treatment over ordered $TiO_2$ nanotubes. LEDs are a promising irradiation source, which allow to reduce power consumption and costs of photocatalytic processes. In this work, a series of $TiO_2$ NTs were fabricated by Ti anodization followed by calcination. The effect of the anodization voltage, electrolyte composition, calcination time and application of ultrasonic treatment before calcination on $TiO_2$ nanotubes morphology (length, diameter and smoothness), photocatalytic activity and photocatalysts stability in four subsequent cycles were investigated.

## 2. Experimental

### 2.1. Materials and instruments

Titanium foil (0.127 mm thickness, 99.7% purity) was purchased from Sigma-Aldrich and used as a Ti substrate for producing ordered $TiO_2$ nanotubes. Isopropanol (p.a., POCh S.A., Poland), acetone and methanol (p.a., P.P.H. STANLAB, Poland) were used for cleaning Ti substrate surface. Sulfuric acid (95%, p.a.), ethylene glycol (99.0%, p.a.), glycerol anhydrous (99.5%, p.a.), ammonium fluoride (p.a.) and hydrofluoric acid (40%, p.a.) were purchased from POCh S.A. (Poland) and used as components for preparation of electrolytes used in Ti anodizing process. Toluene (99.5%, p.a., POCh S.A., Poland) was used as a model air contaminant. All reagents were used without further purification.

The morphology of the resulting $TiO_2$ nanotubes in the form of a thin film was determined by using scanning electron microscopy (SEM) (Quanta 3D FEG, FEI Company). The cross-section images were obtained from the cracked spaces of the samples. Crystal structure of the resulting $TiO_2$ nanotubes photocatalysts was determined from X-Ray diffraction patterns (XRD) measured in the range of $2\theta = 20$–$80°$, using X-ray diffractometer (Xpert PRO-MPD, Philips) with copper $K_\alpha$ radiation ($\lambda = 1.5404$ Å). The XRD estimation of the crystallite size was based on the Scherrer formula:

$$d = \frac{0.9\lambda}{(B_e - B_t)\cos\ \theta}$$

where $\lambda$ is the X-ray wavelength, $B_e$ indicates the measured breadth of a peak profile, while $B_t$ is the ideal, non-broadened breadth of a peak and $\theta$ is the diffraction angle. The value of $B_t$ was estimated on the basis of the measurements performed for the standard sample of polycrystalline Si with large crystalline grains. The accuracy of the grain size analysis has been estimated to be about 20%.

Light-absorption properties of $TiO_2$ nanotubes were characterized by recording diffuse reflectance (DR) spectra and converting the data in order to obtain absorption spectra. The measurements were performed on UV–vis spectrophotometer (Evolution 220, Thermo Scientific) equipped with an integrating sphere. The baseline was determined using barium sulphate as a reference and pure Ti foil.

### 2.2. Preparation of $TiO_2$ nanotubes

The substrate sample (Ti foil, dimensions 2 cm × 3 cm) was ultrasonically cleaned in acetone (10 min), isopropanol (10 min) and methanol (10 min) and subsequently rinsed with deionized water and dried in air. Titanium substrate was anodized in a two-electrode electrochemical set-up, using platinum mesh as a counter electrode as shown in Fig. 1. Ag/AgCl reference electrode was used only for controlling the process and obtaining information about actual potential of Ti working electrode. Three types of electrolyte solutions containing fluoride ions were used in the electrochemical process: (i) water-based electrolyte ($H_2O$, $H_2SO_4$ 1 M, HF 0.1 M), (ii) glycerol-based electrolyte (glycerol 55%, v/v, $H_2O$ 45%, v/v, $NH_4F$ 0.27 M), (iii) ethylene glycol-based electrolyte (ethylene glycol 98%, v/v, $H_2O$ 2%, v/v, $NH_4F$ 0.09 M). Each substrate sample was anodized for 1 h at the applied voltage from the range of 10–40 V using programmable DC power supply (MANSON SDP 2603). The actual current and potential of Ti electrode vs. Ag/AgCl reference electrode was measured and recorded using digital multimeters (BRYMEN BM857a) connected to the computer. Obtained samples were rinsed with deionized water, ultrasonically treated (deionized water, 5 min), dried in air (80 °C for 24 h) and calcinated at 450 °C (heating rate 2 °C/min). The description of all produced samples including their preparation methodology is summarized in Table 1.

### 2.3. Measurement of photocatalytic activity

Photocatalytic activity of prepared $TiO_2$ nanotubes thin films was determined in the process of cleaning air from volatile organic compounds (VOC). Toluene was used as a model air contaminant. The photocatalysts activity tests were carried out in a flat stainless steel reactor with the working volume of about 30 cm$^3$ (see details in Fig. 2). The reactor was equipped with a quartz window, two valves and a septa (Fig. 2a). An array of 25 UV LEDs ($\lambda_{max} = 375$ nm, 63 mW per diode) or 1000 W Xe lamp (OPTEL Opole, Poland) was used as an irradiation source, as shown in Fig. 2c and d. Measured light flux (in the range from 310 to 380 nm) was 11.2 and 17.3 mW/cm$^2$ for LEDs and Xe lamp, respectively (Hamamatsu UV Power meter, model C9536-01). Titanium plate covered by $TiO_2$ nanotubes (2 cm × 2 cm) was placed at the bottom side of the reactor followed by closing the reactor with a quartz window. Subsequently, the gaseous mixture was passed through the reaction space for 2 min. After closing the valves, the reactor was kept in dark for 10 min in order to achieve equilibrium. A reference sample was taken just before starting irradiation. The analysis of toluene concentration in the gas phase was performed using gas chromatograph (Clarus 500, PerkinElmer) equipped with flame ionization detector (FID) and Elite-5 capillary column (30 m × 0.25 mm, 0.25 μm). The samples (200 μl) were dosed by using a gas-tight syringe. By-product formed during toluene irradiation were identified using GC–MS analyses (Shimadzu GCMS-QP2010 Plus chromatograph). A fused-silica capillary column DB-5 MS (60 m × 0.25 mm I.D., 0.5 μm film thickness) from Marchel-Nagel was used. Helium 1 ml/min was used as the carrier gas. The following oven temperature program was used: 5 min at 40 °C, then an increase to 200 °C at rate of 20 °C/min and hold for 3 min. Constant temperatures of 200, 220, and 200 °C were kept at
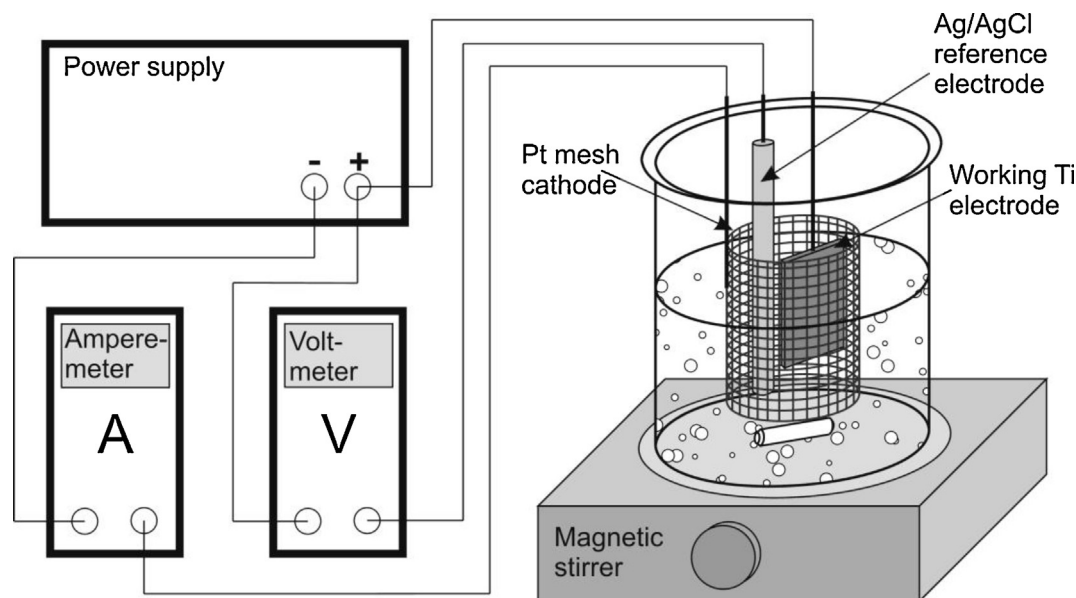
**Fig. 1.** Electrochemical set-up for $TiO_2$ nanotubes preparation.

the ion source, interface, and injector, respectively. 0.5 ml of sample was injected into the GC–MS instrument in the split mode 1:20.

To estimate toluene loss due to adsorption at the photocatalyst surface and direct photolysis, the experiments within the presence of light nor photocatalyst were proceeded. The toluene concentration decreased in the dark experiment of about 4 and 8% after 30 and 60 min, respectively. The toluene loss was not observed during direct irradiation in the absence of photocatalyst.

## 3. Results and discussion

### 3.1. Morphology

Morphology of the prepared samples was investigated by using scanning electron microscopy (SEM). Top view images of the samples prepared by electrochemical oxidation of Ti in different electrolytes are shown in Fig. 3 and the tubes dimensions (diam-

**Table 1**
Preparation methodology of $TiO_2$ nanotubes thin films.

| No. | Sample label[a] | Preparation procedure | | | | |
|-----|-----------------|----------------------|--|--|--|--|
| | | Treatment before anodization | Electrolyte | Anodization parameters | Treatment after anodization | Calcination parameters |
| 1 | NT_Wa_40V_3h | | $H_2O$, $H_2SO_4$ 1 M, HF 0.1 M | 40 V, 1 h | Drying at 80 °C for 24 h | 2 °C/min, 450 °C for 3 h |
| 2 | NT_Gl_40V_3h | | Glycerol 55% (v/v), $H_2O$ 45% (v/v), $NH_4F$ 0.27 M | 40 V, 1 h | Drying at 80 °C for 24 h | 2 °C/min, 450 °C for 3 h |
| 3 | NT_EG_40V_1h | Ultrasonic bath (10 min in acetone, 10 min in | Ethylene glycol 98% (v/v), $H_2O$ 2% (v/v), $NH_4F$ 0.09 M | 40 V, 1 h | Drying at 80 °C for 24 h | 2 °C/min, 450 °C for 1 h |
| 4 | NT_EG_40V_3h | isopropanol, 10 min in methanol), rinsing with | Ethylene glycol 98% (v/v), $H_2O$ 2% (v/v), $NH_4F$ 0.09 M | 40 V, 1 h | Drying at 80 °C for 24 h | 2 °C/min, 450 °C for 3 h |
| 5 | NT_EG_40V_6h | deionized water, air drying | Ethylene glycol 98% (v/v), $H_2O$ 2% (v/v), $NH_4F$ 0.09 M | 40 V, 1 h | Drying at 80 °C for 24 h | 2 °C/min, 450 °C for 6 h |
| 6 | NT_EG_40V_US_1h | | Ethylene glycol 98% (v/v), $H_2O$ 2% (v/v), $NH_4F$ 0.09 M | 40 V, 1 h | Ultrasonic bath (5 min in deionized water), drying at 80 °C for 24 h | 2 °C/min, 450 °C for 1 h |
| 7 | NT_EG_40V_US_3h | | Ethylene glycol 98% (v/v), $H_2O$ 2% (v/v), $NH_4F$ 0.09 M | 40 V, 1 h | Ultrasonic bath (5 min in deionized water), drying at 80 °C for 24 h | 2 °C/min, 450 °C for 3 h |
| 8 | NT_EG_40V_US_6h | | Ethylene glycol 98% (v/v), $H_2O$ 2% (v/v), $NH_4F$ 0.09 M | 40 V, 1 h | Ultrasonic bath (5 min in deionized water), drying at 80 °C for 24 h | 2 °C/min, 450 °C for 6 h |
| 9 | NT_EG_30V_US_6h | | Ethylene glycol 98% (v/v), $H_2O$ 2% (v/v), $NH_4F$ 0.09 M | 30 V, 1 h | Ultrasonic bath (5 min in deionized water), drying at 80 °C for 24 h | 2 °C/min, 450 °C for 6 h |
| 10 | NT_EG_20V_US_6h | | Ethylene glycol 98% (v/v), $H_2O$ 2% (v/v), $NH_4F$ 0.09 M | 20 V, 1 h | Ultrasonic bath (5 min in deionized water), drying at 80 °C for 24 h | 2 °C/min, 450 °C for 6 h |
| 11 | NT_EG_10V_US_6h | | Ethylene glycol 98% (v/v), $H_2O$ 2% (v/v), $NH_4F$ 0.09 M | 10 V, 1 h | Ultrasonic bath (5 min in deionized water), drying at 80 °C for 24 h | 2 °C/min, 450 °C for 6 h |

[a] NT, nanotubes; Wa, water-based electrolyte; Gl, glycerol-based electrolyte; EG, ethylene glycol-based electrolyte; 10–40 V, anodization voltage; US, sample ultrasonically treated after anodization; 3–6 h, calcination time.
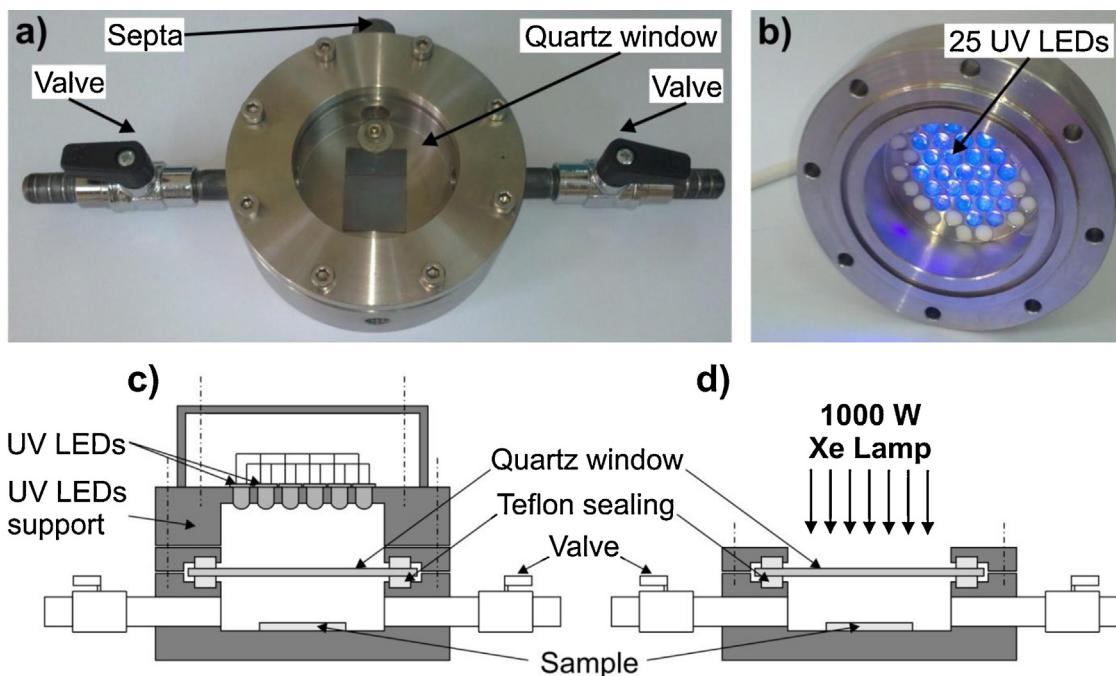
**Fig. 2.** Photocatalytic set-up for gas phase reaction: (a) image of gas phase photoreactor; (b) image of UV LEDs array; (c) scheme of photoreactor equipped with UV LEDs as an irradiation source; and (d) scheme of photoreactor equipped with 1000 W Xe lamp as an irradiation source.

eter, length and wall thickness) based on SEM images are given in Table 2. All samples were anodized for 1 h with applied voltage of 40 V and annealed in 450 °C for 3 h with heating rate 2 °C/min. TiO$_2$ nanotubes obtained from glycerol-based electrolyte (Fig. 3a) have a well-exposed surface with a small amount of impurities.

The tubes' diameter is approximately equal to 200 nm but it should be noticed that these nanotubes are not smooth and consist of a large number of uneven rings arranged one upon the other. On the other hand, the nanotubes prepared with ethylene glycol-based electrolyte (Fig. 3b) are more uniform and smooth but their surface
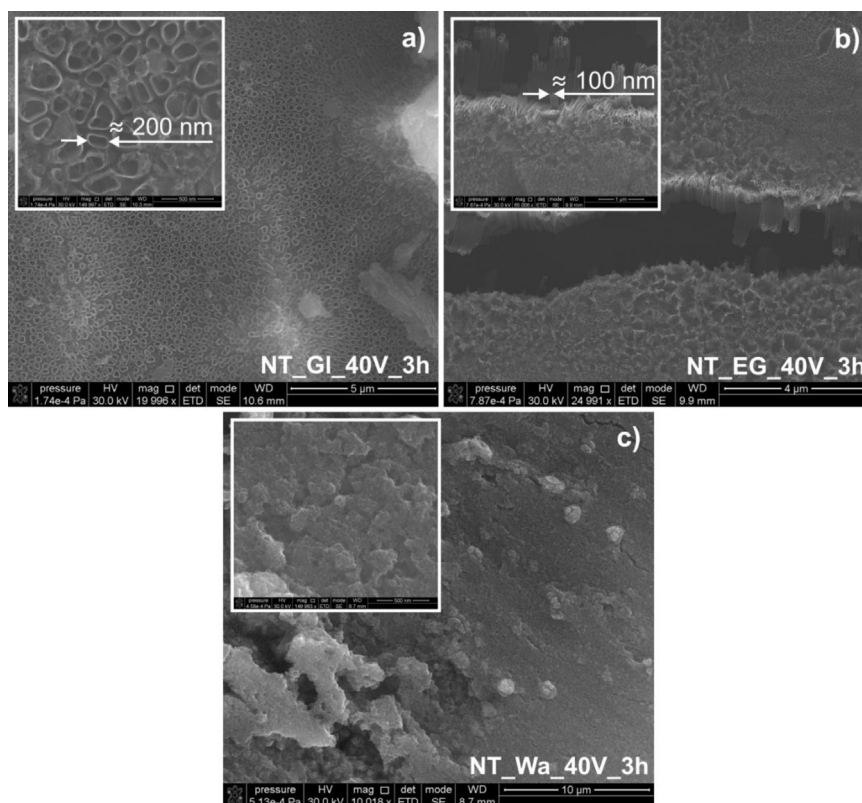


**Fig. 3.** The influence of electrolyte composition on the morphology of the resulting thin TiO$_2$ films: (a) glycerol-based electrolyte, (b) ethylene glycol-based electrolyte, (c) water-based electrolyte.

**Table 2**
Dimensions of TiO$_2$ nanotube arrays formed in ethylene glycol-based electrolyte (based on SEM images).



| Sample label | Nanotubes diameter, $d$ [nm] | Approximated nanotubes length, $l$ [μm] | Approximated wall thickness, $b$ [nm] | Estimated outer surface area of single TiO$_2$ tube [nm$^2$] | Estimated inner surface area of single TiO$_2$ tube [nm$^2$] | Estimated total surface area of single TiO$_2$ tube [nm$^2$] |
|---|---|---|---|---|---|---|
| NT_Gl_40V_3h | 219 | 0.9 | 16 | $619 \times 10^3$ | $528 \times 10^3$ | $1147 \times 10^3$ |
| NT_EG_40V_3h | 102 | 5.1 | 24 | $1633 \times 10^3$ | $865 \times 10^3$ | $2498 \times 10^3$ |
| NT_EG_10V_US_6h | 31 | 0.5 | 10 | $49 \times 10^3$ | $17 \times 10^3$ | $66 \times 10^3$ |
| NT_EG_20V_US_6h | 63 | 1.8 | 13 | $356 \times 10^3$ | $209 \times 10^3$ | $565 \times 10^3$ |
| NT_EG_30V_US_6h | 84 | 4.3 | 17 | $1134 \times 10^3$ | $675 \times 10^3$ | $1810 \times 10^3$ |
| NT_EG_40V_US_6h | 110 | 5.9 | 25 | $2038 \times 10^3$ | $1112 \times 10^3$ | $3150 \times 10^3$ |

is covered with impurities consisting of hydrous titanium oxides created as a consequence of hydrolysis of TiO$_2$ during anodization [29]. The outer diameter of the nanotubes prepared with ethylene glycol-based electrolyte is equal to about 100 nm and it is half the size of the nanotubes prepared using glycerol-based electrolyte. However, nanotubes formed in glycerol-based electrolyte are much shorter that than one prepared in ethylene glycol-based solution (see details in Table 2). Tubes length differed from about 0.9 to 5.1 μm using glycerol and ethylene glycol, respectively. Fig. 3c shows the surface of the sample anodized in water-based electrolyte. The resulting TiO$_2$ thin film does not have the structure of nanotubes. Referring to Ghicov et al. [30] nanotubes should occur in the case of applying anodization voltage of 20 V. Thin layer structure strictly depends on anodization parameters such as electrolyte composition and applied voltage [31] and when the voltage exceeds an optimal value, nanotubes change into porous, sponge-like structure as in the case of the sample presented in Fig. 3c.

The surface of ordered NTs, in the case of using organic-based electrolyte, is crashed, not flat and in some cases contaminated. Crashes in the resulting layer and differences in nanotubes' length are the consequences of the creases and roughness of Ti substrate which was covered with oxide layer before anodization [17] and are not easy to avoid. Nevertheless, the contaminants can be easily removed from the NTs' surface by treating the sample with ultrasonic waves after the anodization process. Fig. 4a shows the sample anodized in ethylene-glycol-based electrolyte for 1 h, applying 40 V and subsequently calcined in 450 °C for 6 h with heating rate 2 °C/min. Fig. 4b presents the sample prepared analogously, but applying ultrasonic bath for 5 min just after anodization. It can be seen, that ultrasonically treated sample is free of surface contamination, nanotubes are open and easily accessible to light irradiation and reagents in photocatalytic reaction.

The dimensions of TiO$_2$ NTs can be easily controlled in a wide range by changing the applied voltage. Fig. 5 shows SEM images of the samples anodized in ethylene glycol-based electrolyte for 1 h, ultrasonically treated and calcined for 6 h with heating rate

2 °C/min. Fig. 5a–d correspond to nanotubes obtained by applying anodization voltage from the range of 10–40 V. Tubes' diameter and length increases approximately linearly with the applied voltage for this range, starting from about $d$ = 31 nm and $l$ = 0.5 μm (10 V) and reaching about $d$ = 110 nm and $l$ = 5.9 μm (40 V), see details in Table 2. Nanotubes obtained with higher voltages are more uniform, longer and their surface is smoother as compared to nanotubes obtained with lower voltages.

The effect of electrolyte type on the morphology of TiO$_2$ nanotube arrays is schematically presented in Fig. 6. It was shown that the morphology and the structure of nanotubular/nanoporous TiO$_2$ layer are affected strongly by the solution parameters, such as fluoride ions concentration, pH and water content in the electrolyte [32]. As reported by the Macak et al. [33], the anodic growth of compact oxides on metal surfaces and the formation of tubes are governed by a competition between anodic oxide formation and chemical dissolution of the oxide as soluble fluoride complexes. Fast nanotube growths rates are also determined between a balance of water and fluoride concentration [33]. High fluoride concentration enhances the dissolution of TiO$_2$ (TiO$_2$ + 6F$^-$ + 4H$^+$ → [TiF$_6$]$^{2-}$ + 2H$_2$O) while addition of water allows for a sufficient rate of titanium oxidation (Ti + O$_2$ → TiO$_2$). Usually, titania nanotubes with smooth walls are grown using viscous solvents for anodization [34]. Solvent with high viscosity reduce the mobility of fluoride ions and other ionic species reducing the growth rate, but also reducing current fluctuations and therefore forming smoother nanotube walls. In our experiments, nanotubes with smoother walls were obtained in almost water free, ethylene glycol-based, electrolyte (see Fig. 6a). Macak et al. [34] demonstrated that the water content significantly influence on the wall morphology. In case of organic electrolyte with water content high enough to behave as aqueous, the periodically repeated differences in the dissolution and oxide formation rate cause to leave some parts of the wall thicker and the other thinner, those leading to side walls ripples [34].
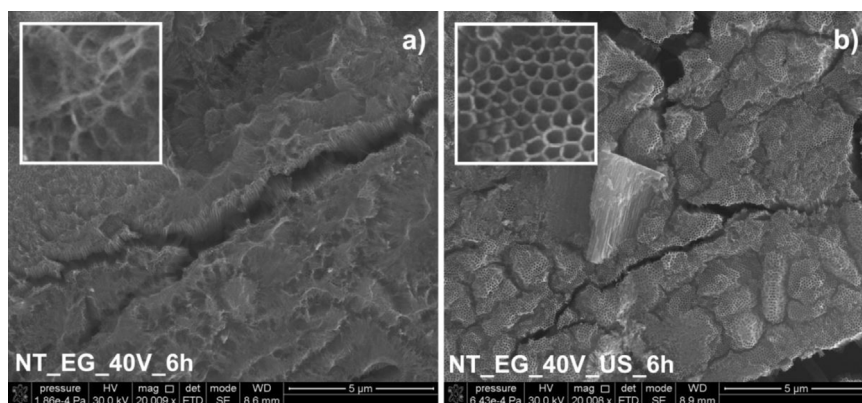
**Fig. 4.** The influence of ultrasonic treatment on the surface morphology of the resulting thin $TiO_2$ films.

Ethylene glycol-based electrolyte had slightly higher viscosity than a glycerol-based one (13.1 and 11.8 cP, respectively) and according to our expectations, nanotubes arrays formed in ethylene glycol-based electrolyte have a smooth walls. Whereas nanotubes obtained in glycerol-based electrolyte are not smooth and consist of a large number of uneven rings arranged one upon the other as shown in Fig. 6b. It could be assumed, that in glycerol-based electrolyte, the nanotubes wall morphology have been affected by high water content (45 vol.% $H_2O$) in the electrolyte. Lower viscosity of electrolyte and relatively higher rate of chemical dissolution of $TiO_2$ caused to formation of the ripples.

Usually, $TiO_2$ nanotube arrays, growing in HF electrolytes or acidic HF mixture, showed a limited thickness that not exceed 500–600 nm. Ordered nanotubes in water-based electrolyte (containing HF) has been commonly formed at low voltages (below 25 V) [32]. Thus, in case of relatively high voltage (40 V) application, compact oxide layer was formed instead of ordered nanotubes

(Fig. 6c). Our observation confirmed report of others [31,35] as with increasing of applied voltage to 30 V, nanotubular structure were destroyed and nanotube surface layer changed to a porous, sponge-like structure (Fig. 6c).

### 3.2. XRD analysis

Fig. 7 presents the results of X-ray diffraction measurements for the samples obtained with the use of ethylene glycol-based electrolyte, anodizing voltage between 10 V and 40 V, ultrasonic treatment before calcination and calcination temperature of 450 °C. For comparison, the pattern of the Ti substrate is also shown in Fig. 7a. All the patterns consist of the reflexes corresponding to the anatase form of $TiO_2$ and/or to the Ti the substrate. Letter R marks the position of the main rutile reflex ($2\theta = 27.5°$), where in the patterns of the samples anodized at voltage below 40 V a small and wide bump can be seen. It may be attributed to the transformation
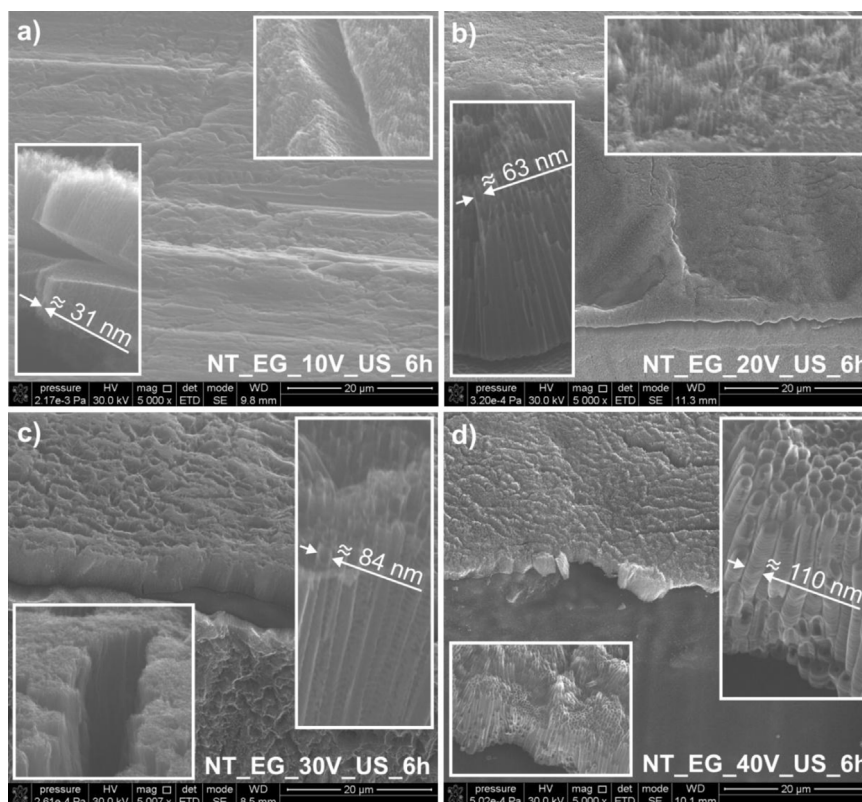


**Fig. 5.** SEM images of $TiO_2$ nanotubes prepared via Ti anodization in the ethylene glycol-based electrolyte at different voltages: 10, 20, 30 and 40 V.
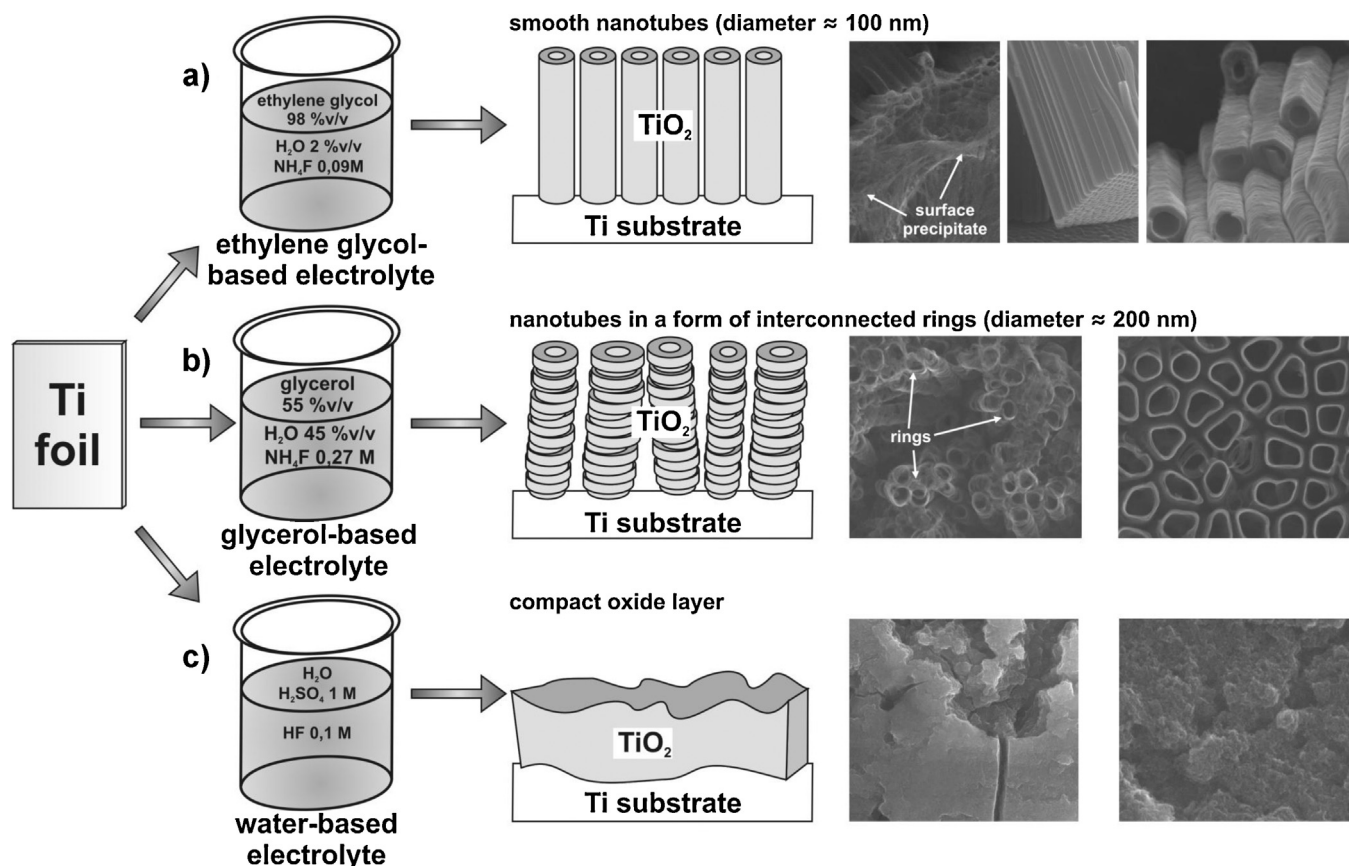
**Fig. 6.** The effect of electrolyte type on the morphology of $TiO_2$ nanotube arrays.

of the anatase to rutile in the interfacial region between the nanotubes and the Ti substrate, which may occur at 430–450 °C [34]. It can be seen that the intensity of the anatase reflexes increase while these of the substrate decrease with the increase of anodizing voltage (Fig. 7a) and calcination time (Fig. 7b). It is caused by growing thickness of the nanotube layer. All patterns show the ratio of relative intensity of (0 0 4) and (1 0 1) reflexes much larger than 0.2 which is expected for isotropic polycrystalline anatase. It indicates that the nanotubes are partially ordered and their growth direction is along the [0 0 1] direction. It should be noted

that the XRD pattern of the sample anodized at 40 V and calcined at 450 °C for 6 h (NT_EG_40V_US_6h) reveals the highest, equal to 3, ratio of (0 0 4) and (1 0 1) reflexes intensities, which means that the nanotubes on this sample surface are most ordered. Fig. 7b illustrates the influence of the calcination time on the nanotube structure. The "as received" layers which were not subjected to the heat treatment are amorphous. The crystallization occurs during the calcination. It can be seen that calcination influences the intensity, the intensity ratio and the width of the (1 0 1) and (0 0 4) reflexes of anatase. The average crystallite size of our samples
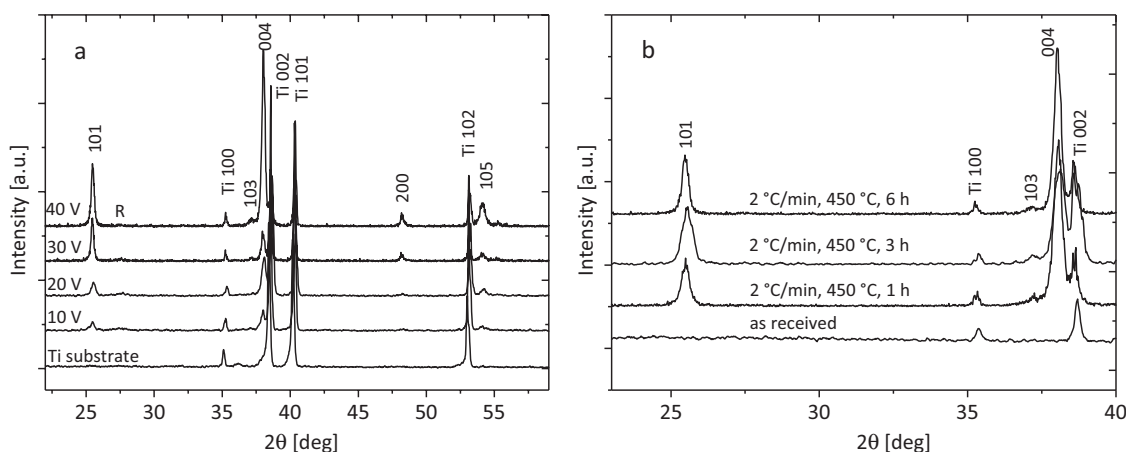


**Fig. 7.** The XRD patterns for the samples obtained with the use of ethylene glycol-based electrolyte, anodized and calcined in different conditions. Fig. 8a shows the results obtained for anodizing at 10, 20, 30 and 40 V followed by the calcination at 450 °C for 6 h. The patterns shown in Fig. 8b correspond to the samples anodized at 40 V and: not calcined, calcined and calcined at 450 °C for 3 h and for 6 h. The reflexes marked by Miller indices correspond to anatase, by Ti and Miller indices–to the substrate. Letter R marks the position of the main rutile reflex ($2\theta = 27.5°$).

(treated in ethylene glycol-based electrolyte with different voltage followed by calcination, 450 °C for 6 h), increased from $40 \pm 5$ to $60 \pm 5$ nm with increasing voltage from 10 to 40 V, respectively. It was also observed, that 6 h calcination leads to formation of larger crystallites in the tube wall compared with 3 h thermal treatment. Increase in calcination time from 1 to 6 h caused increase of average crystallite size up from 30 to 40 nm up to $60 \pm 5$ nm, respectively. According to the literature data, the structure of the as grown oxide can be amorphous or crystalline and it strongly dependent on the specific electrochemical parameters, such as the applied potential, the time of anodization, or the sweep rate of the potential ramp. For example, the structure of the oxide film on $TiO_2$ has typically been reported to be amorphous at low voltages (below 20 V) and crystallization to take place at higher voltages. Depending on the anodization conditions the crystal structure has been reported to be anatase, a mixture of anatase rutile or rutile [32]. In our case, while the higher voltages (40 V) have been applied, obtained $TiO_2$ nanotubes have amorphous structure.

### 3.2.1. UV–vis properties

Fig. 8 shows the UV–vis absorption spectra of $TiO_2$ nanotubes prepared at different anodization voltages. All samples were anodized in ethylene glycol-based electrolyte for 1 h, ultrasonically treated and calcined at 450 °C for 6 h with heating rate 2 °C/min. It can be seen, that for all samples the minimum reflectance occurs in the UV region. Sharp reflectance edges occur at the wavelength of about 350 nm, except for the sample anodized in 10 V with a sharp
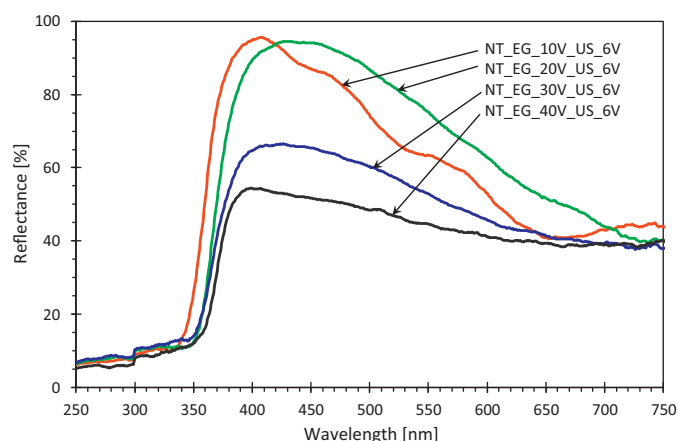


**Fig. 8.** Diffuse reflectance spectra of $TiO_2$ nanotubes prepared at different anodization voltages.

reflectance edge at about 340 nm. Nanotubes prepared by anodization of Ti at 10 V and 20 V show nearly 100% reflectance in the visible region of shorter wavelengths. In comparison, nanotubes prepared at higher voltages have the maximum reflectance at the range of 65% and 55% for the samples anodized at 30 V and 40 V respectively. Reflectance value in the UV region is similar for all samples. It suggests that even the thinnest film, which was prepared at 10 V,
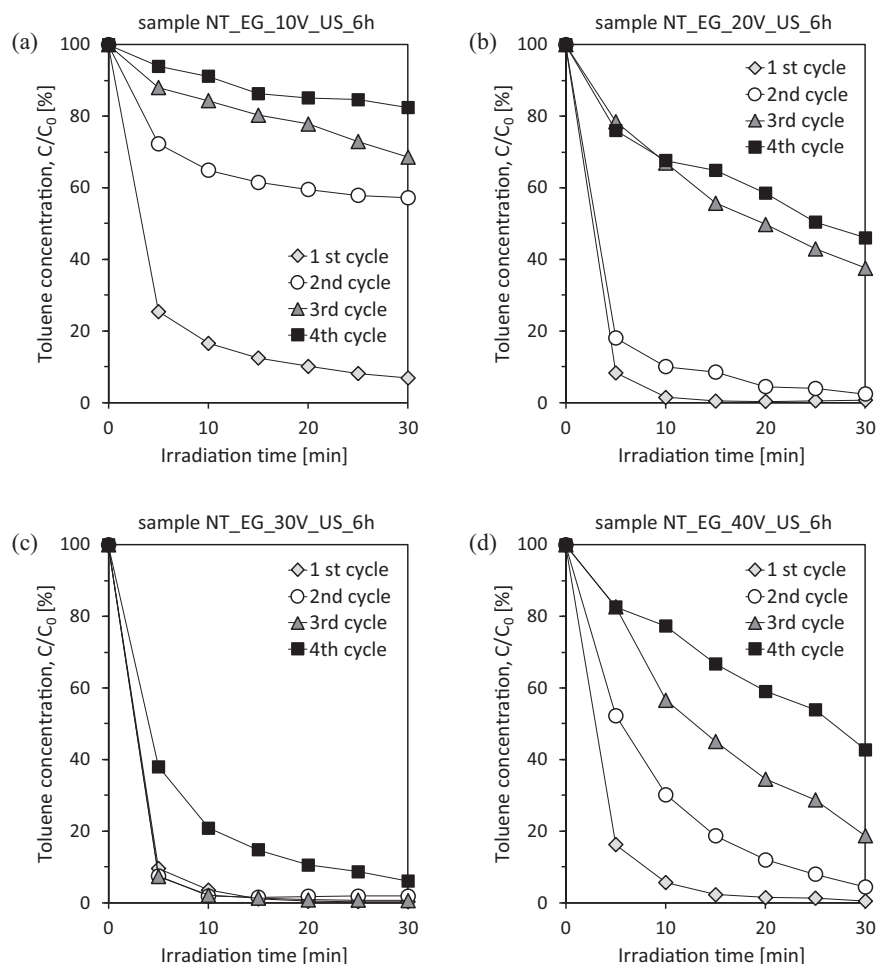


**Fig. 9.** Toluene photodegradation efficiency as the function of irradiation time. The influence of anodization voltage on the initial photocatalytic activity of $TiO_2$ nanotubes and their stability in four measurement cycles under Xe lamp irradiation.
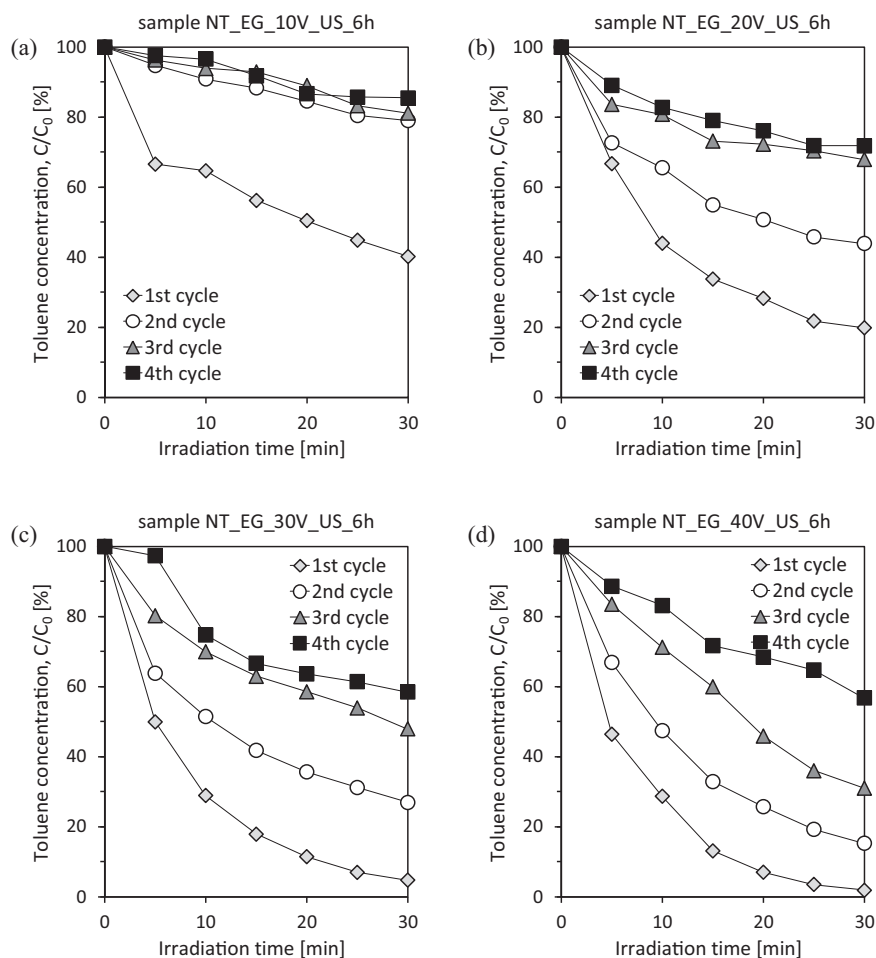
**Fig. 10.** Toluene photodegradation efficiency as the function of irradiation time. The influence of anodization voltage on the initial photocatalytic activity of $TiO_2$ nanotubes and their stability in four measurement cycles under UV LEDs irradiation.

covers the Ti substrate surface completely. Otherwise, titanium metal reflectance will be observed in UV region [28].

### 3.3. Photocatalytic degradation of toluene

The effect of applied voltage on the initial photocatalytic activity of $TiO_2$ nanotubes as well as their stability in four measurement cycles under UV using 1000 W Xe lamp were presented in Fig. 9. All these samples were anodized in ethylene glycol-based electrolyte for 1 h, ultrasonically treated and calcined at 450 °C for 6 h with heating rate 2 °C/min. The samples anodized at 20 and 30 V showed the highest photocatalytic activity in the first measurement cycles, since only about 10% of initial toluene amount remained after 5 min of irradiation. The sample anodized at 40 V showed slightly lower activity, as degradation efficiency after 5 min of irradiation reached about 80%. However, in the case of these three samples all toluene was removed from gas phase after 30 min irradiation, e.g. the final toluene concentration was below detection limit. In the case of nanotubes prepared at 10 V toluene removal efficiency reached about 90% after a 30-min process and was much lower in comparison to the samples prepared at higher voltages. The photocatalysts' activity decreased in subsequent measurement cycles which suggests that active sides of $TiO_2$ may have been blocked by toluene partial decomposition products. Definitely, the biggest decrease in activity was observed in the case of nanotubes anodized at 10 V (only 20% degradation of toluene in the fourth measurement cycle). The sample anodized at 30 V was the most stable.

Experiments were repeated using lower power irradiation source (UV LEDs array). In these conditions, toluene degradation rate was lower (Fig. 10), however in the case of the samples anodized at 30 and 40 V reached near 100% after 30 min in the first cycle. In the next cycles, as in the case of Xe lamp, the activity of photocatalysts decreased, i.e. the efficiency of toluene removal over nanotubes formed at 10 V reached only 20% in the second cycle. In the case of using UV LEDs as irradiation source (in contrast to Xe lamp), the samples anodized at 30 V and 40 V behaved similarly. 60-min irradiation resulted in about 40% toluene degradation the fourth cycle. $CO_2$ formation during irradiation of toluene in the gas phase over $TiO_2$ nanotube arrays, using xenon lamp and light-emitting diodes, was confirmed using GC–MS technique. Carbon dioxide concentration was increased with the decrease of toluene content.

Photocatalytic properties of anodized $TiO_2$ nanotubes depend not only on anodization voltage (and resulting dimensions) but also on the treatment after electrochemical process, such as calcination time and ultrasonic cleaning before calcination (Fig. 11). All samples were anodized at 40 V for 1 h, ultrasonically treated (or left without ultrasonic treatment) and calcined at 450 °C (heating rate 2 °C/min) for 1, 3, and 6 h respectively. Photocatalytic activity was measured in toluene removal process under UV LEDs irradiation. Studies showed, that ultrasonic treatment significantly increased photocatalysts' stability in several measurement cycles. This suggests, that impurities created on the nanotubes' surface during anodization process are largely responsible for the decrease of photocatalytic activity.
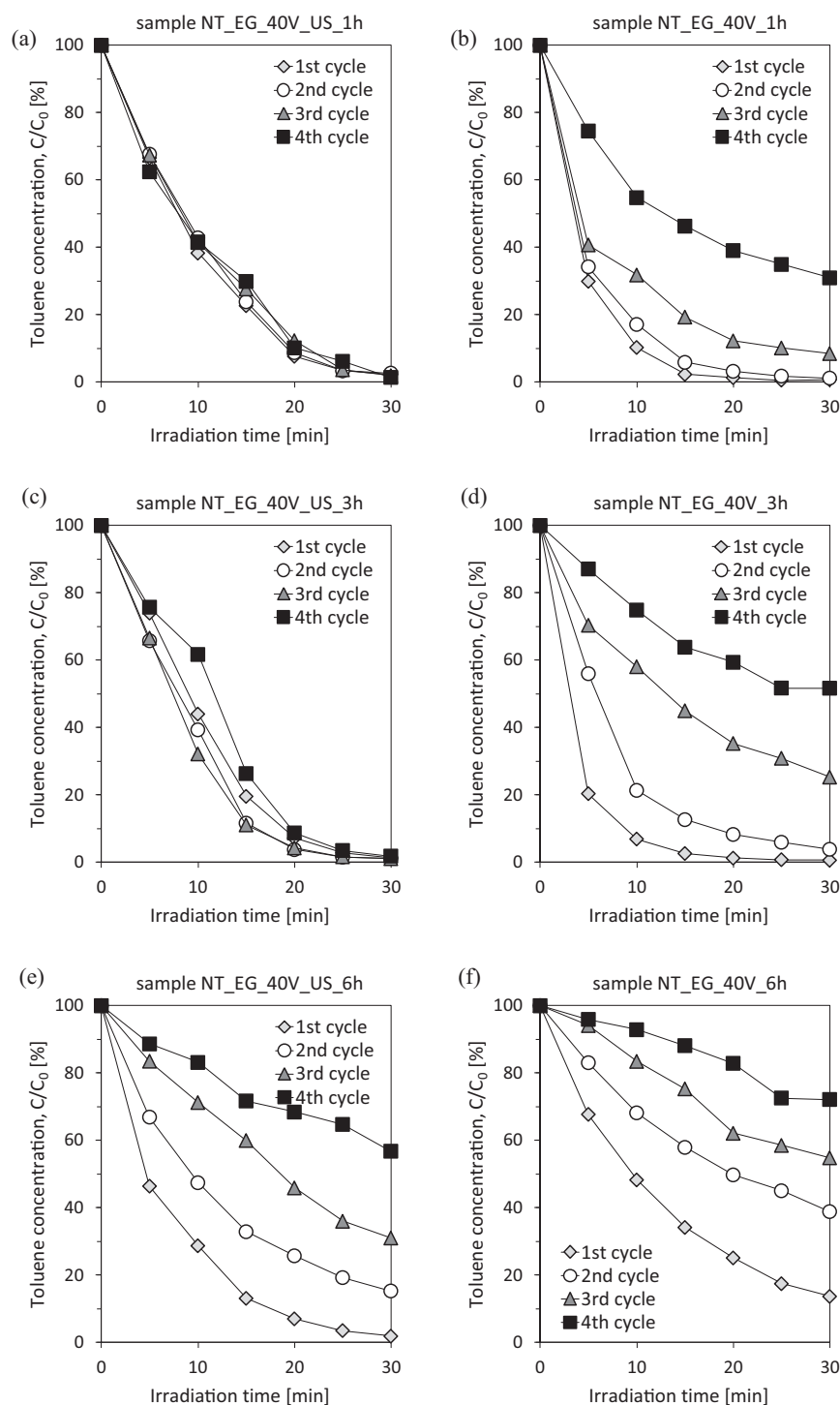
**Fig. 11.** Toluene photodegradation efficiency as the function of irradiation time. The influence of calcination time on the initial photocatalytic activity of TiO$_2$ nanotubes and their stability in four measurement cycles under UV LEDs irradiation. Plots on the left side represent samples ultrasonically treated before calcination while plots on the right side represent samples without ultrasonic treatment.

The activity and stability of TiO$_2$ nanotubes also depend on the duration of heat treatment. Ultrasonically treated and calcined (1 h or 3 h) samples did not lose their photocatalytic properties in the fourth measurement cycles. In the case of the sample calcined for 6 h, the loss of activity was significant. As previously mentioned, the longer the calcination time is, the bigger crystallites of TiO$_2$ are formed. This may suggest, that titania nanotubes which are calcined for a shorter time (and are composed of smaller crystallites) are more suitable material for photocatalytic air treatment.

It is know that the photoresponse is dominated by two competitive factors: (1) the effect of nanotubes length on light absorption (the longer the tubes, the higher the total light absorption); and (2) the effect of nanotubes length on electron-holes recombination process (the longer the tubes, the higher the recombination losses). The optimum tube length (for UV conversion) was found about 1 μm (depending on the wavelength) [36]. Calculated surface area of single TiO$_2$ tube formed in ethylene glycol-based electrolyte (based on SEM images) are shown in Table 2. The tubes lengths
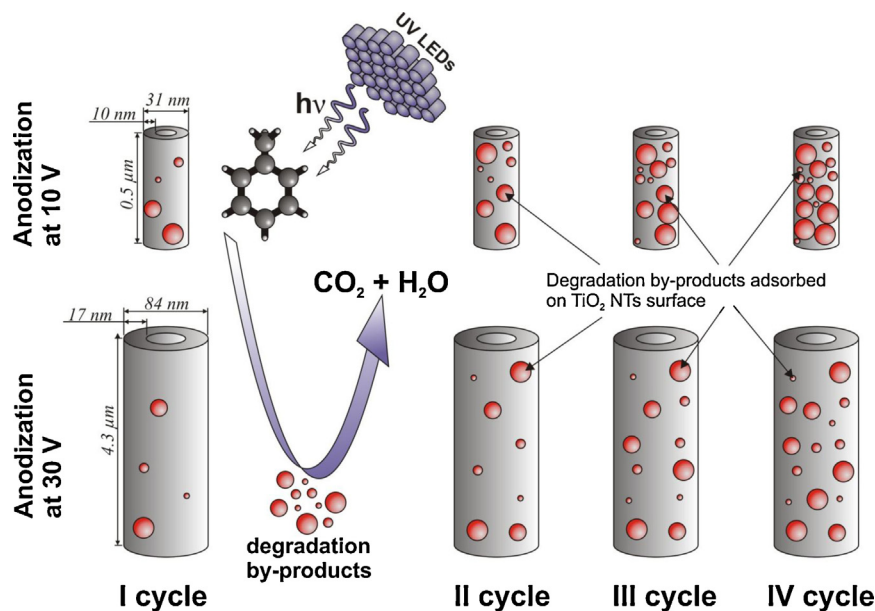
**Fig. 12.** Schematic illustration of the nanotube surface blocking by adsorbed by-products formed during toluene photodegradation.

varied from 0.5 to 5.9 μm and the wall thickness from 10 to 25 nm for applied anodization voltage from 10 to 40 V, respectively. Since the xenon lamp was used for toluene degradation over TNT, not too much difference in degradation efficiency was observed for tubes differed in lengths from 0.5 to 5.9 μm in the first cycle of the reaction. However, the highest photoactivity in four subsequent cycles was observed in case of 4.3-μm-long tubes. Lower efficiency of toluene degradation in subsequent cycles could be a result of TiO$_2$ nanotubes surface blocking by adsorbed toluene degradation byproducts, as shown in Fig. 12. The 0.5-μm-long nanotube arrays and 1.8-μm-long nanotube arrays having much smaller surface area, lose photoactivity due to faster surface filling by adsorbed by-products molecules. To evidence if lower photoactivity really resulted from blocking a surface by degradation products, used samples were irradiated by high powered UV lamp (to clean the surface) and re-use in toluene degradation reaction. Increase in photoactivity in toluene degradation was observed for re-irradiated samples (results are not shown). Thus, the TiO$_2$ NTs no-reproducibility does not result from film instability but probably from blocking the surface by degradation by-products.

The difference between toluene photodegradation in four subsequent cycles over 4.3-μm-long and 5.9-μm-long tubes is insignificant. Although surface area of single 5.9-μm-long tube is almost twice bigger than surface area of single 4.3-μm-long tube, total surface area of 4.3-μm-long and 5.9-μm-long nanotube arrays is probably similar due to different number of nanotubes per Ti foil surface unit resulted from different nanotubes diameter. Enhancing the photoactivity for increasing the lengths of nanotube arrays in some range was also observed by Liu et al. [26]. Increasing the lengths of nanotube arrays from 0.2 to 17 μm accelerated the degradation rate of acetaldehyde in gas phase significantly. But further increasing the length of nanotube array to 27 μm did not further improve the photocatalytic activity. They concluded, that at a specific length, limited by the extinction depth of UV light and/or diffusion depth of pollutants molecules in the TiO$_2$ nanotube array, the photocatalytic activity will reach a plateau. Photocatalytic activity of the TiO$_2$ nanotube arrays was evaluated by photodegradation of methyl orange after 5 h UV irradiation by Sreekantan et al. [37]. They found that Ti foil anodized at 5 V showed very poor degradation as compared to Ti foil anodized at 20 and 30 V. Among them, Ti foil anodized at 20 V showed the highest photoactivity in

methyl orange degradation process. They claimed that this sample has large surface area due to the tubular structure and more reactants could be adsorbed onto inner and outer surfaces of the tubes and thus favor higher photocatalytic activity. As for Ti foil anodized at 30 V, the diameter is larger and the wall thickness is thicker. Due to this the surface area is reduced and hence the photocatalytic degradation is also reduced. Thus, thin walls are another structural characteristics of TiO$_2$ nanotubes and these structural features reduce the recombination of holes and electrons generated by photo-absorption because the half-thickness of the nanotube wall is significantly less than the carrier diffusion length in TiO$_2$ [38].

Since the LEDs (emitting irradiation with wavelength of 375 nm) were used, the highest photoactivity in the first cycle of toluene degradation was observed for 4.3-μm-long and 5.9-μm-long nanotube arrays. It could be assumed that in case of xenon lamp, the high flux of irradiated light causes that the effect of absorbed light is probably irrelevant. However, when the light-emitting diodes were used (low-intensity light), the bigger nanotube surface area related to higher length of tubes, resulted in better absorption of light and observed higher toluene degradation efficiency. Bigger surface of tubes could also resulted in higher adsorption capacity toward toluene degradation by-products. In case of shorter tubes (0.5 and 1.8 μm), smaller nanotubes surface could be filled by adsorbates faster, resulting in rapid decrease in photoefficiency in subsequent cycles as shown in Fig. 10. Further increased in photoactivity could be obtained by affecting the TNT structure by shortening calcinations process (see Fig. 11).

## 4. Conclusions

In summary, photocatalytic activity of TiO$_2$ NTs in the gas phase reaction strictly depend on nanotubes morphology (length of tubes, top-opened or clogged and wall smoothness). The highest photoactivity in toluene degradation reaction was observed for longer (4.3-μm- and 5.9-μm-long nanotube arrays) obtained by Ti-foil anodization in ethylene glycol-based electrolyte. Prolonged calcination steps resulted in decrease of photoactivity due to increase of crystallite size and appearance of rutile phase. It was shown that TiO$_2$ nanotube arrays are effective in gas phase treatment using low powered irradiation sources, e.g. LEDs.

30-min of irradiation by twenty five UV-LEDs ($\lambda_{max}$ = 375 nm, 63 mW per diode) was enough to complete removal of toluene ($C_0$ = 100 ppm) from the gas phase in the presence of $TiO_2$ nanotube arrays formed in ethylene glycol-based electrolyte at 30 V, followed by ultrasound treatment and 1 h calcinations at 450 °C. The same photoactivity was observed in four subsequent cycles. For NTs obtained in another reaction conditions, photoactivity was lowered in subsequent cycles probably due to adsorption of toluene degradation by-products at tubes surface. Photoactivity could be re-established by extended UV irradiation.

Although the total light flux intensity emitted by 25 LEDs array is less than emitted by Xe lamp (11.2 and 17.3 mW/cm$^2$ for LEDs and Xe lamp, respectively), efficiency of gas phase treatment over $TiO_2$ nanotubes was comparable for both irradiation sources. Nevertheless, power consumption of 25 diodes array was only 1.575 W compared to 1000 W for Xe lamp. Thus, $TiO_2$ nanotubes ordered arrays are a promising photocatalytic material that are relatively easy to synthesize and by further optimization of its preparation conditions it may be practically applied in the air purification processes using energy efficient light sources [39].

## Acknowledgement

## References

[1] N. Doucet, F. Bocquillon, O. Zahraa, M. Bouchy, Chemosphere 65 (2006) 1188–1196.
[2] F. Shiraishi, T. Ishimatsu, Chemical Engineering Science 64 (2009) 2466–2472.
[3] N.R. Neti, G.R. Parmar, S. Bakardjieva, J. Subrt, Chemical Engineering Journal 163 (2010) 219–229.
[4] F.-L. Toma, L.M. Berger, D. Jacquet, D. Wicky, I. Villaluenga, Y.R. de Miguel, J.S. Lindeløv, Surface and Coatings Technology 203 (2009) 2150–2156.
[5] C.H. Ao, S.C. Lee, J.C. Yu, Journal of Photochemistry and Photobiology A: Chemistry 156 (2003) 171–177.
[6] W. Chen, J.S. Zhang, Building and Environment 43 (2008) 246–252.
[7] S. Josset, S. Hajiesmailia, D. Begina, D. Edouarda, C. Pham-Huua, M.-C. Lett, N. Kellera, V. Kellera, Journal of Hazardous Materials 175 (2010) 372–381.
[8] Y. Paz, Applied Catalysis B: Environmental 99 (2010) 448–460.
[9] A. Zaleska, A. Hänel, M. Nischk, Recent Patents on Engineering 4 (2010) 200–216.
[10] J. Taranto, D. Frochot, P. Pichat, Separation and Purification Technology 67 (2009) 187–193.
[11] C. Sarantopoulos, E. Puzenat, C. Guillard, J.-M. Herrmann, A.N. Gleizes, F. Maury, Applied Catalysis B: Environmental 91 (2009) 225–233.
[12] M. Altomare, M. Pozzi, M. Allieta, L.G. Bettini, E. Selli, Applied Catalysis B 136/137 (2013) 81–88.
[13] S. Bauer, A. Pittrof, H. Tsuchiya, P. Schmuki, Electrochemistry Communications 13 (2011) 538–541.
[14] P. Roy, S. Berger, P. Schmuki, Angewandte Chemie International Edition 50 (2011) 2904–2939.
[15] Y. Sun, G. Wang, K. Yan, International Journal of Hydrogen Energy 36 (2011) 15502–15508.
[16] A. Harring, A. Morris, M. Hu, Materials 5 (2012) 1890–1909.
[17] Z. Zhang, Md. F. Hossain, T. Takahashi, International Journal of Hydrogen Energy 35 (2010) 8528–8535.
[18] S.K. Mohapatra, N. Kondamudi, S. Banerjee, M. Misra, Langmuir 24 (2008) 11276–11281.
[19] Z. Liu, B. Pesic, K.S. Raja, R.R. Rangarajua, M. Misra, International Journal of Hydrogen Energy 34 (2009) 3250–3257.
[20] D. Kowalski, P. Schmuki, Chemical Communications 46 (2010) 8585–8587.
[21] P.M. Perillo, D.F. Rodríguez, Sensors and Actuators B 171/172 (2012) 639–643.
[22] J.M. Macak, M. Zlamal, J. Krysa, P. Schmuki, Small 3 (2007) 300–304.
[23] C. Das, P. Roy, M. Yang, H. Jha, P. Schmuki, Nanoscale 3 (2011) 3094–3096.
[24] M. Yang, D. Kim, H. Jha, K. Lee, J. Paul, P. Schmuki, Chemical Communications (2011) 2032–2034.
[25] M. Altomare, K. Lee, M.S. Killian, E. Selli, P. Schmuki, Chemistry – A European Journal 19 (2013) 5841–5844.
[26] Z. Liu, X. Zhang, S. Nishimoto, T. Murakami, A. Fujishima, Environmental Science & Technology 42 (2008) 8547–8551.
[27] A.G. Kontos, A. Katsanaki, T. Maggos, V. Likodimos, A. Ghicov, D. Kim, J. Kunze, C. Vasilakos, P. Schmuki, P. Falaras, Chemical Physics Letters 490 (2010) 58–62.
[28] A.G. Kontos, A. Katsanaki, V. Likodimos, T. Maggos, D. Kim, C. Vasilakos, D.D. Dionysiou, P. Schmuki, P. Falaras, Chemical Engineering Journal 179 (2012) 151–157.
[29] H. Xu, Q. Zhang, C. Zheng, W. Yan, W. Chu, Applied Surface Science 257 (2011) 8478–8480.
[30] A. Ghicov, J.M. Macak, H. Tsuchiya, J. Kunze, V. Haeublein, L. Frey, P. Schmuki, Nano Letters 5 (2006) 1080–1082.
[31] H. Omidvar, S. Goodarzi, A. Seif, A.R. Azadmehr, Superlattices and Microstructures 50 (2011) 26–39.
[32] J.M. Macak, H. Tsuchiya, A. Ghicov, K. Yasuda, R. Hahn, S. Bauer, P. Schuki, Current Opinion in Solid State & Materials Science 11 (2007) 3–18.
[33] J.M. Macak, H. Tsuchiya, P. Schmuki, Angewandte Chemie International Edition 44 (2005) 2100–2102.
[34] J.M. Macak, H. Hildebrand, U. Marten-Jahns, P. Schmuki, Journal of Electroanalytical Chemistry 621 (2008) 254–266.
[35] D.J. Yang, H.G. Kim, S.J. Cho, W.Y. Choi, Materials Letters 62 (2008) 775–779.
[36] J.M. Macak, M. Zlaman, J. Krysa, P. Schmuki, Small 3 (2007) 300–304.
[37] S. Sreekantan, R. Hazan, Z. Lockman, Thin Solid Films 518 (2009) 16–21.
[38] K. Nakata, A. Fujishima, Journal of Photochemistry and Photobiology C 13 (2012) 169–189.
[39] W. Dytrych, M.A. Zaleska Nischk, A. Zielińska-Jurek, A. Cybula, A. Gołębiewska, J. Reszczyńska, M. Klein, E. Grabowska, Method of making of materials with photocatalytic and biocidal properties containing ordered TiO2 nanotube array modified with metals, particularly noble metals (in Polish), Pat. Apl. P401627 (2012).